Detection of melamine based on the suppressed anodic response of uric acid by a Au−Ag nanoparticles modified glassy carbon electrode

Yu-Hui Peng [a], Tsunghsueh Wu [b,*], Yang-Wei Lin [a,**]

[a] Department of Chemistry, National Changhua University of Education, 1 Jin-De Road, Changhua City, 50007, Taiwan
[b] Department of Chemistry, University of Wisconsin-Platteville, 1 University Plaza, Platteville, WI, 53818-3099, USA

Abstract

We demonstrated a sensitive electrochemical method for the determination of nonelectroactive melamine (Mel) using a modified glassy carbon electrode (GCE), with uric acid (UA) as the signal reporter. To increase the anodic response of UA, GCE was coated with Au−Ag nanoparticles and a Nafion thin film (Au−Ag/Nafion/GCE). The sensing mechanism was based on the competitive adsorption behavior of Mel on the Au−Ag/Nafion/GCE, which reduces the electroactive surface area of nanoparticles and thus hinders anodic response of UA. Under optimal conditions and the use of an analytical method of differential pulse voltammetry, this modified electrode detected Mel concentrations ranging from 2.5 to 70 nM, with a detection limit of 1.8 nM. The Au−Ag/Nafion/GCE demonstrated satisfactory reproducibility and stability, with relative standard deviations (RSDs) of 9.3% and 7.1%, respectively. The proposed electrochemical method was then successfully used to determine the Mel content in spiked milk powder and cat food samples, with RSDs of 1.7%−9.3% and recoveries of 92.4%−103.7%.

Keywords: Au−Ag NPs, Differential pulse voltammetry, Melamine, Nafion, Uric acid

1. Introduction

Adulteration of milk powder with melamine (Mel) has caused infant fatality and hospitalization and was a critical food safety concern in 2008 [1]. Melamine powder has a similar appearance to that of milk powder and possesses a high nitrogen content (66% nitrogen by mass), similar to that of proteins. Therefore, Mel is intentionally adulterated to milk products by unethical manufacturers to falsely increase protein concentration. Consumption of Mel-contaminated milk products causes urinary system damage, kidney stones, and death because of the formation of insoluble high molecular weight Mel-complexes in renal tubules [1]. Accordingly, the US Food and Drug Administration (FDA) set the maximum level of Mel in food products at 20.0 μM (2.5 ppm) to ensure food safety. Several instrumental methods have been developed for the detection and estimation of Mel, such as colorimetric assay, enzyme-linked immunosorbent assay, fluorescence spectroscopy, surface-enhanced Raman spectroscopy, capillary electrophoresis−mass spectrometry, and liquid chromatography−mass spectrometry [2−9]. Although these methods produce accurate and precise results, they are expensive to employ, time consuming, and require tedious sample preparation [10−21]. Furthermore, they cannot be employed for rapid on-site analysis [22].

Electrochemical methods offer numerous advantages because of their inexpensive, simplicity, and high detecting performance compared with existing

Received 3 May 2020; accepted 30 June 2020.
Available online 28 August 2020.

* Corresponding author.

** Corresponding author.
E-mail addresses: wut@uwplatt.edu (T. Wu), linywjerry@cc.ncue.edu.tw (Y.-W. Lin).

https://doi.org/10.38212/2224-6614.1075

methods [23]. Unfortunately, Mel is poor electroactive and highly stable; thus, few studies have performed direct electroanalysis of Mel. Several indirect electrochemical methods were developed to improve the electroactivity of Mel. For example, Li et al. described an electrochemical DNA-based sensor for real-time measurement of Mel in flowing milk [24]. The DNA sensors are based on thiol-anchored DNA sequences, comprising two polythymine segments connected by a four-cytosine loop with a redox reporter. The sensor responds to changes in melamine concentration within seconds without contaminating the product stream by using melamine-induced DNA triplex formation to generate an electrochemical output. Liu et al. developed a sensitive homogeneous electroanalytical platform for Mel detection, which relies on the formation of a triplex molecular beacon integrated with exonuclease III–mediated signal amplification [25]. This sensing platform uses the high binding affinity of the DNA triplex structure with Mel and the unique features of exonuclease III for sensitive and selective Mel assay, with a limit of detection (LOD) as low as 8.7 nM. Although DNA-modified electrochemical sensors are sensitive and save time, the design of DNA sequences and their chemical modification with redox reporters and immobilization processes are complex and expensive. Regasa et al. proposed a family of molecularly imprinted copolymer thin films, such as polyaniline, poly(aniline-*co*-itaconic acid), and poly(aniline *co*-acrylic acid), deposited on a glassy carbon electrode (GCE) using an in situ electropolymerization method with Mel as a template [26–28]. The electron conductivity of polyaniline films increased with increasing Mel concentrations in the sample solution from the electroactivity of Mel. Furthermore, the delocalization of charges formed acceptor-type sites and caused an increase in $[Fe(CN)_6]^{3-/4-}$ electron transfer rates as the quantity of Mel increased. After the rebinding of Mel, the proposed sensors provided excellent LODs (0.4 nM–17.9 pM) with high selectivity. However, the preparation of these polyaniline-based conductive films is lab intensive and time consuming.

Metal- and nonmetal-nanocomposite–modified GCEs have been used for Mel detection because their unique electronic and catalytic properties are ideal for signal generation and transduction in sensing [29]. For example, Daizy et al. proposed the electrochemical detection of Mel by using a reduced graphene oxide-copper nanoflower modified GCE [30]. Under optimal conditions, the proposed method can detect Mel concentrations ranging from 10 to 90 nM with a LOD of 5.0 nM. Peng et al. suggested the sensitive electrochemical detection of Mel by using gold nanoparticles (Au NPs) deposited on a graphene-doped carbon paste electrode [31]. The sensing mechanism is based on the interaction between melamine and the Au NPs, causing suppression of the peak current. The proposed method exhibited a satisfactory linear relationship in the concentration range of 0.2–800 nM, with a LOD of 0.18 pM. Furthermore, Ren proposed a competitive immunosensor based on polyethyleneimine functionalized reduced graphene oxide and a Au NP–modified electrode for the detection of Mel [32]. Mel was determined using differential pulse voltammetry (DPV) in a buffer solution containing $[Fe(CN)_6]^{3-/4-}$. This Mel immunosensor exhibited a linear relationship in the concentration range of 1 pM to 1 μM, with a LOD of 0.27 pM. Although metal- and nonmetal-nanocomposite–modified electrochemical sensors provide superior sensitivity, the fabrication of a nanocomposite-modified electrode is complicated. Therefore, developing a simple and convenient fabrication procedure for nanocomposite-modified electrodes with high selectivity and sensitivity is crucial.

In this study, we propose a simple procedure to fabricate modified GCE and detect Mel by using an indirect electrochemical method. A GCE was coated sequentially with a drop of Au–Ag NP solution, which was synthesized in HEPES buffer at room temperature. A Nafion thin film was then used to secure the Au–Ag NPs on the electrode surface. The Nafion film was used to coat the modified GCE surface because of its unique ionic conductivity and excellent thermal and mechanical stability. For simplicity, this sensing electrode is denoted as Au–Ag/Nafion/GCE. Through hydrophobic interaction, Mel preferentially adsorbs onto Au–Ag NPs, blocking the electroactive surface to the adsorption of the signal reporter (i.e., uric acid [UA]) in the standard solution and thus suppressing the anodic current from UA. On the basis of this mechanism, we constructed an electrochemical method for the detection of Mel using Au–Ag/Nafion/GCE with UA as a signal reporter for milk powder and animal food analysis.

2. Experiment

2.1. Chemicals

All chemicals were purchased from Sigma–Aldrich (Milwaukee, WI, USA). All the reagents were commercially available and of analytical reagent grade, including $HAuCl_4$, $AgNO_3$, KCl, NaCl, $CaCl_2$, $MgCl_2$, NaH_2PO_4, Na_2HPO_4, Na_3PO_4, HEPES, UA, Mel, $Ru(NH_3)_6^{2+}$, Nafion, ammonia, phenylamine, glucose, sucrose, lactose, fructose, glycine, adenine, and thymine. NaH_2PO_4, Na_2HPO_4,

and Na_3PO_4 were used to prepare phosphate buffer (PB) solutions at different pH values to use as the electrolyte solutions. Ultrapure water (18.2 MΩ cm) from a Milli-Q ultrapure system (Millipore, MA, USA) was used.

2.2. Preparation of Au–Ag NPs

Au–Ag NPs were synthesized by mixing 10 μL of 0.4 mM $AgNO_3$ and 90 μL of 0.4 mM $HAuCl_4$ in 100 μL of 200 mM HEPES solution at room temperature. The mixed solution was pipetted five times by using a 100 μL micropipette and left to grow in the dark. After 24-hr incubation, the color of the solution had changed from light yellow to red, indicating the formation of Au–Ag NPs. The prepared Au–Ag NPs were washed three times following centrifugation-washing procedures (8000 rpm, 10 min) with ultrapure water. The concentration of the prepared Au–Ag NPs was defined as 1 × .

2.3. Fabrication of a Au–Ag/Nafion-modified GCE

The base of the GCE (4 mm in diameter) was polished successively with 1 and 0.05 μm alumina slurry before modification. After each round of polishing, it was rinsed with ultrapure water, sonicated in ethanol for 5 min, and then sonicated in ultrapure water for 5 min. Finally, after it was dried under nitrogen flow, it was ready for use.

A 5-μL drop of 1 × Au–Ag NP solution was added to the GCE surface, which was then dried in a vacuum dryer at room temperature. A polymer with ionic conductivity, Nafion (0.5%, 2 μL), was coated on the modified GCE surface to secure Au–Ag NPs on the GCE. The Au–Ag/Nafion/GCE sensor was fabricated in 10 min using premade Au–Ag and Nafion solutions.

2.4. Characterization of Au–Ag NPs

A JEOL 2010 transmission electron microscope (TEM, JEOL, Tokyo, Japan) with an acceleration voltage of 200 kV was used to study the morphologies of the prepared Au–Ag NPs in the absence and presence of UA and Mel. An Evolution 200 UV–Vis spectrometer (ThermoFisher, NY, USA) was used to record the UV–Vis spectra of the prepared Au–Ag NP solutions in the absence and presence of UA and Mel. A dynamic light scattering spectrophotometer (DLS, ELSZ-2000ZS, Otsuka Electronics Co., Ltd., Osaka city, Japan) was used to measure the hydrodynamic diameter and zeta potential of the prepared Au–Ag NPs in the absence and presence of UA and Mel.

2.5. Electrochemical apparatus

Cyclic voltammetry (CV) and DPV experiments were performed at the CHI 600 electrochemical workstation (CH Instruments, Austin, TX, USA). A conventional three-electrode system was used, consisting of a Au–Ag/Nafion/GCE working electrode, a platinum wire auxiliary electrode, and a Ag/AgCl reference electrode. All experiments were performed at 25 ± 1 °C. DPV experiments were performed at a scan rate of 20 mV/s with a 50-mV pulse amplitude, 50-ms pulse width, and 250-ms pulse period.

2.6. Pre-treatment of milk powder and cat food sample

0.2 g milk powder and cat food purchased from local supermarket were mixed with 25 mL methanol solution containing 0.01 M trichloroacetic acid. After 20 min stirring, the solution was purified through centrifugation at 12,000 rpm for 10 min, and the supernatant was filtered. Then, the filtrate was condensed to get a total volume of 5 mL and filtered using a 0.2–μm filter membrane.

3. Results and discussion

3.1. Sensing scheme

The effects of analytes on Au–Ag NPs were initially investigated in the solution phase. Fig. 1A summarizes the study of analyte–nanoparticle interaction from the UV–Vis spectrum of the prepared Au–Ag NPs in the absence and presence of analyte solutions. As the black curve in Fig. 1A illustrates, the prepared Au–Ag NPs exhibited a surface plasmon resonance (SPR) absorption peak at 520 nm. The TEM image in Fig. 1B reveals that the diameter of the prepared Au–Ag NPs was 20.1 ± 2.7 nm. The prepared Au–Ag NPs were stable without coagulation for at least 1 month when stored at room temperature in the dark, as verified by both TEM and UV–Vis measurements after storage. The findings further demonstrated that the SPR bands of the prepared Au–Ag NPs for three different batches of Au–Ag NPs were reproducible (relative standard deviation [RSD] < 2.13%) for sensor development. Following a reported colorimetric assay for Mel detection based on the hydrophobic interaction of

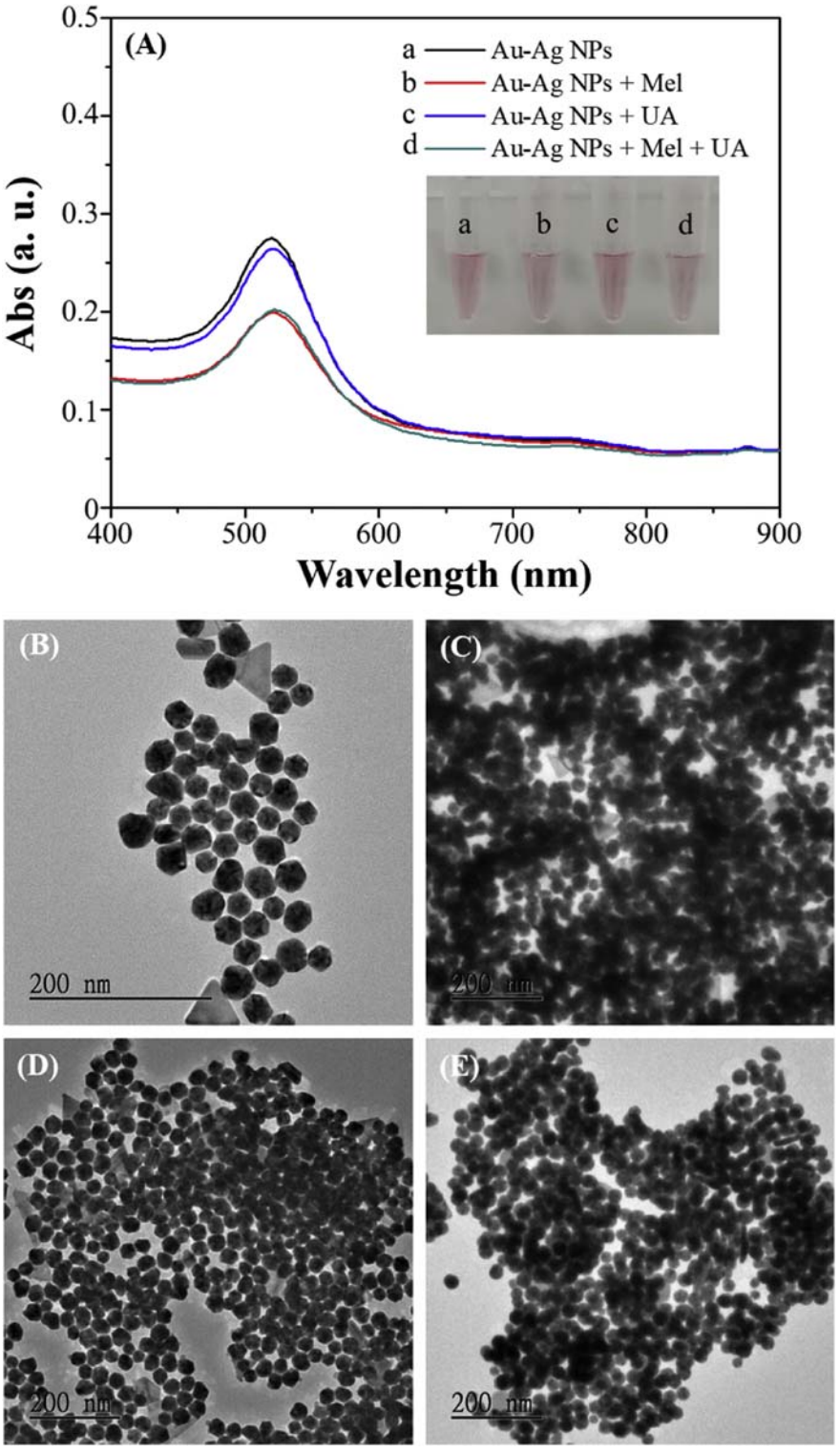

Fig. 1. (A) UV–Vis spectra of 0.5 × Au–Ag NPs (a, black), 0.5 × Au–Ag NPs + 0.25 mM Mel (b, red), 0.5 × Au–Ag NPs + 0.25 mM UA (c, blue), and 0.5 × Au–Ag NPs + UA + Mel (both 0.25 mM, d, green). TEM images of (B) Au–Ag NPs, (C) Au–Ag NPs + Mel, (D) Au–Ag NPs + UA, and (E) Au–Ag NPs + Mel + UA. The scale bar for all TEM images is 200 nm.

citrate stabilized Au NPs [29], Mel (0.5 mM, 200 μL) was added to the prepared Au–Ag NP solution (1 ×, 200 μL) and measured using UV–Vis, the results of which are represented by the red curve in Fig. 1A. The SPR band wavelength and intensity of the prepared Au–Ag NPs in the presence of Mel redshifted slightly to 526 nm, and the absorbance was reduced by 27.6%, indicating that Mel induced aggregation of Au–Ag NPs. The TEM image displayed in Fig. 1C confirmed the aggregation of Au–Ag NPs in the presence of Mel. From our observation, the color change when comparing the color of the Au–Ag NP solution in the absence and presence of Mel was not obvious, suggesting that the Au–Ag NPs were unsuitable for colorimetric assay (inset image in Fig. 1A).

Our analytical method was based on a competitive adsorptive strategy as an indirect approach to measuring Mel. Investigating the interaction of Au–Ag NPs with Mel along with that of the Au–Ag NPs with the reporter is crucial. For the development of this sensor, Mel should interact strongly with the Au–Ag NPs, whereas the reporter should have a small or negligible interaction with the Au–Ag NPs. As mentioned, UA was selected as a reporter molecule for current transduction in our sensor. The observed analyte–nanoparticle interaction is illustrated in Fig. 1A; Mel can interact with Au–Ag NP in a solution. The addition of UA at a quantity (0.5 mM, 200 μL) comparable to that of Mel into the Au–Ag NP solution did not influence the absorption wavelength of the nanoparticles. Furthermore, when Mel and UA were added to the Au–Ag NPs, the UV–Vis spectra for the mixture of Mel and UA were similar to those of Mel alone. These results strongly indicate that Mel can preferentially adsorb Au–Ag NPs, causing a particle aggregation that is more prominent than that for UA. The nanoparticle aggregates from the mixture of Mel and UA were studied under TEM, as illustrated in Fig. 1E. Table 1 summarizes the hydrodynamic diameters and zeta potentials of the prepared Au–Ag NPs in the absence and presence of Mel and UA. The hydrodynamic diameter and zeta potential of the prepared Au–Ag NPs in the presence of Mel and UA were larger and less negative, respectively, than for the free-Au–AgNPs, which contributed to the induced aggregation and shielded partial negative charge of Au–Ag NPs, predominantly in the presence of Mel.

Table 1. Hydrodynamic diameter and zeta potential of the prepared Au–Ag NPs under different conditions.

Samples	Hydrodynamic diameter (nm)	zeta potential (mV)
Au–Ag NPs	25.5 ± 0.4	−47.25 ± 0.86
Au–Ag NPs + Mel	46.2 ± 0.4	−24.61 ± 0.67
Au–Ag NPs + Mel + UA	30.5 ± 0.1	−44.23 ± 0.49

After the preferential interaction of Mel on the surface of Au–Ag NPs was realized, an electrochemical assay for the detection of Mel by using Au–Ag/Nafion/GCE was conducted, as illustrated in Scheme 1. An Au–Ag NP solution (5 μL) was added to the base of GCE, followed by a Nafion film coating, to secure nanoparticles on the modified GCE surface. The modified GCE was then immersed in a solution containing only UA and a PB solution, and a significant anodic oxidation current of UA was produced at 0.34 V. However, the anodic current of UA was decreased in the presence of Mel because Mel adsorbed on the prepared Au–Ag/Nafion/GCE surface, thus reducing the electroactive surface area and suppressing the electrooxidation of UA.

The electrochemical behavior of the proposed method was characterized in detail. Fig. 2A illustrates the cyclic voltammograms in the absence and presence of Mel and UA (both 1.0 mM) on the Au–Ag/Nafion/GCE. The red curve in Fig. 2A represents an anodic peak of UA produced on the Au–Ag/Nafion/GCE when it was scanned anodically. The anodic current of UA, represented by the blue curve in Fig. 2A, was significantly suppressed after the addition of Mel to the same UA testing solution and did not cause a dilution effect. The peak potential did not shift significantly, suggesting that the electrochemical process is caused by the oxidation of UA and not a side reaction. The reduction in anodic current may be caused by the reduction in the transport of UA to the electrode surface. Therefore, the transport characteristics of UA were further studied by changing the scan rate of CV. As illustrated in the inset in Fig. 2B, the anodic current responses of UA were determined to be linearly related to the scan rate, indicating an adsorption-controlled process on the Au–Ag/Nafion/GCE. The mechanism of the oxidation of UA involves the intermediate formation of a Au–N interaction before the electron transfer from UA to nanoparticles, and this Au–N interaction was disrupted and blocked by the presence of the Mel. These findings indicate that the hydrophobic interaction between Au–Ag NPs and Mel noticeably reduced the number of Au sites available for reaction with UA. Therefore, the anodic peak of UA on the Au–Ag/Nafion/GCE was suppressed after the addition of Mel.

The electroactive molecule $Ru(NH_3)_6^{2+}$ was used to confirm that the suppressed current was related to

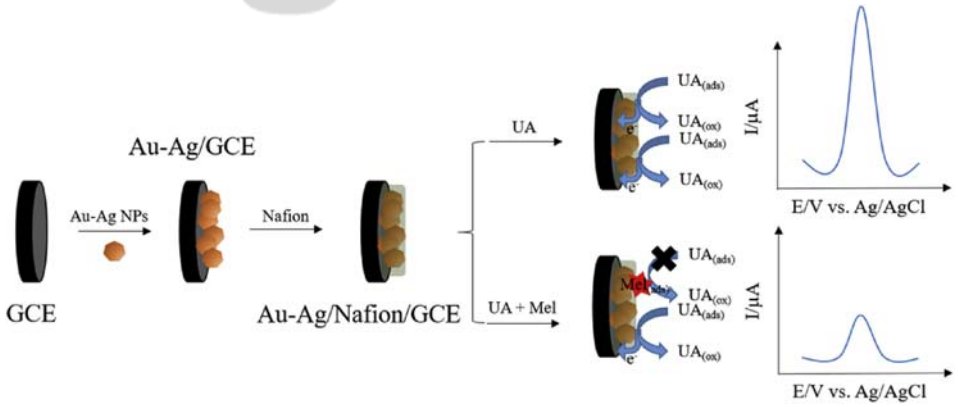

Scheme 1. Schematic of the mechanism for the electrochemical detection of Mel by using a Au–Ag/Nafion/GCE.

the adsorption of UA and Mel at the Au–AgNP/Nafion/GCE. Fig. 3A illustrates the cyclic voltammograms of $Ru(NH_3)_6^{2+}$ in the absence and presence of UA and Mel. We observed a well-defined reversible peak at −0.2 V for $Ru(NH_3)_6^{2+}$ on the Au–AgNP/Nafion/GCE. The reduction in peak current of $Ru(NH_3)_6^{2+}$ could be observed in the presence of UA and Mel, with a larger reduction in

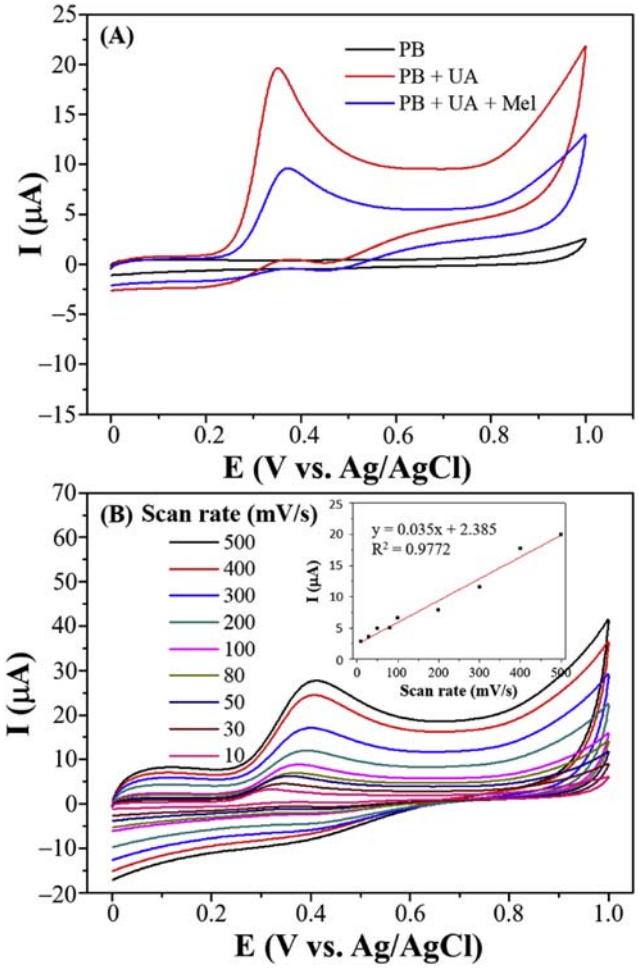

Fig. 2. (A) Cyclic voltammograms of the 50 mM PB solution (pH 7.0, black), 50 mM PB solution + 1.0 mM UA (red), and 50 mM PB solution + 1.0 mM Mel + 1.0 mM UA (blue) on the Au–Ag/Nafion/GCE. (B) Cyclic voltammograms of 50 mM PB (pH 7.0) in the presence of Mel and UA (both 1.00 mM) at different scan rates. Inset: linear plot of current vs. scan rate.

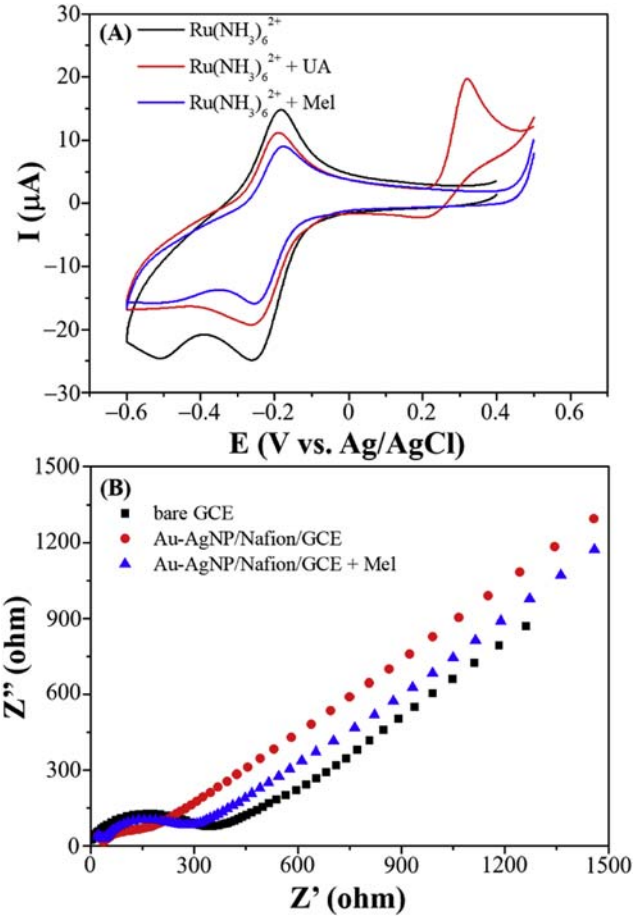

Fig. 3. (A) Cyclic voltammograms of 1.0 mM $Ru(NH_3)_6^{2+}$ (black), 1.0 mM $Ru(NH_3)_6^{2+}$ + 1.0 mM UA (red), and 1.0 mM $Ru(NH_3)_6^{2+}$ + 1.0 mM Mel (blue) on the Au–Ag/Nafion/GCE. (B) EIS of the bare GCE (black), Au–Ag/Nafion/GCE (red), and Au–Ag/Nafion/GCE + 1.0 mM Mel in 5.0 mM $K_3[Fe(CN)_6]$ containing 0.1 M KCl.

the presence of Mel compared with that of UA. As expected, the anodic peak observed at 0.32 V in Fig. 3A corresponds to the oxidation of UA (similar to the peak potential on the red curve in Fig. 2A), and no anodic peak was observed in the Mel solution. Therefore, the reduction in peak current of $Ru(NH_3)_6^{2+}$ was caused by a reduction in the electroactive area of the nanoparticles because of the adsorption of UA and Mel.

Electrochemical impedance spectroscopy (EIS) was used to measure the interfacial properties of the modified GCE. The semicircle diameter at higher frequencies corresponds to the charge transfer resistance. Fig. 3B shows the EIS of the bare GCE and Au–AgNP/Nafion/GCE in a solution of 5.0 mM $K_3[Fe(CN)_6]$ and 0.1 M KCl without and with Mel. The EIS of the bare GCE with a large semicircle was found (black). When Au–AgNPs and Nafion were modified on the GCE surface, the resistance was decreased (red), which was a strong proof that the Au–AgNPs and Nafion were excellent electric conductive materials that accelerated the charge transfer. Subsequently, when the Au–AgNP/Nafion/GCE was in a solution of 5.0 mM $K_3[Fe(CN)_6]$ and 0.1 M KCl containing Mel, the resistance was increased (blue), because Mel inhibited the charge transfer between the redox probe and the electrode, which suggested that Mel was strongly adsorbed on the Au–AgNP/Nafion/GCE surface.

3.2. Optimal conditions

Additional assay parameters were evaluated to further optimize electrochemical detection. The effect of the Ag^+:Au^{3+} molar ratio in Au–Ag NP synthesis was tested over ranges of 5–30 (Fig. 4A) and compared with the relative anodic current variation determined by the formula $(I_0 - I)/I_0$, where I_0 and I are the anodic current of UA (1.0 mM) in the absence and presence of Mel (1.0 mM), respectively. The bar chart in Fig. 4A illustrates that the peak current variation reached its maximum at an Ag^+ to Au^{3+} molar ratio of 10, corresponding to the Ag–Au ratio for maximum sensitivity to Mel. A higher silver ratio corresponds to greater sensitivity of Mel detection. Ag components in Au–Ag NPs are believed to correspond to higher charge transport during the oxidation of UA, but quantities of Ag over 10-fold higher than that of Au could lead to the loss of adsorption sites for Mel, thus increasing the anodic current of UA. Therefore, a molar ratio of Ag^+ to Au^{3+} of 10 was selected as the optimal condition for further investigation.

The volume of Au–Ag NP solution dispensed on the GCE may affect the performance of this sensor because the electroactive area varies with particle loading. Deposition solutions ranging from 2 to 7 μL (Fig. 4B) were also tested, which revealed that the anodic current variation peaked at 5 μL. This result is attributed to the saturated surface coverage of

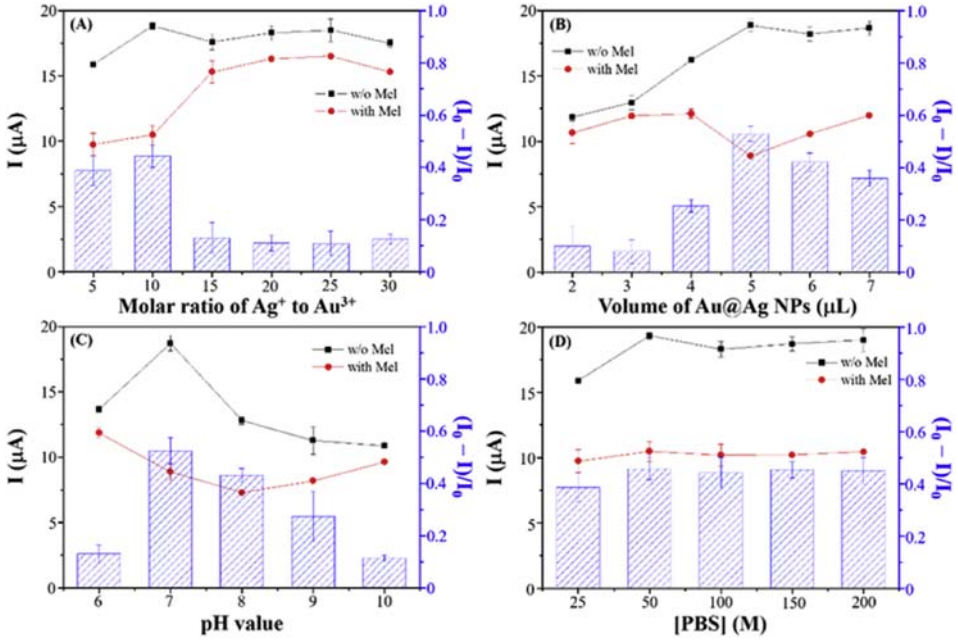

Fig. 4. Optimization of the Au–Ag/Nafion/GCE to determine Mel quantity. (A) Molar ratio of Ag^+ to Au^{3+}, (B) volume of Au–Ag NPs, (C) pH value, and (D) concentration of PB solutions. The error bars represent the standard deviations for triplicate experiments.

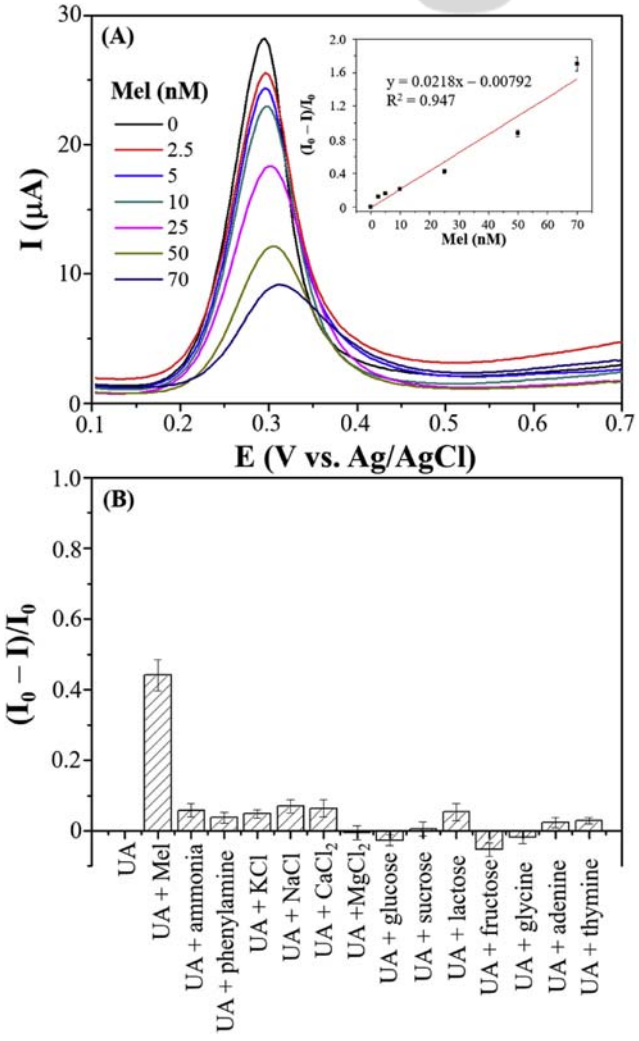

Fig. 5. (A) DPV responses of various concentrations of Mel in a 50 mM PB solution (pH 7.0) with 100 nM UA as the electroactive element. DPV conditions: pulse potential = 50 mV, pulse width = 50 ms, pulse interval = 250 ms. Inset: the difference in the peak current of the Au–Ag/Nafion/GCE at different Mel concentrations. (B) The selectivity of the Au–Ag/Nafion/GCE for Mel. Error bars represent the standard deviations for triplicate experiments.

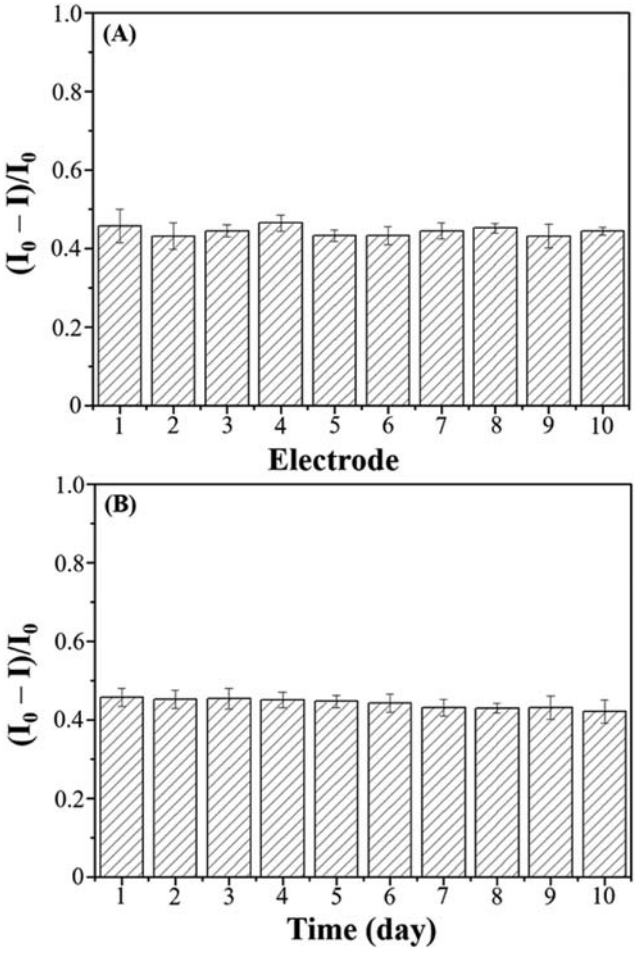

Fig. 6. (A) Reproducibility test: current variation for UA (1.0 mM) by using 10 pieces of Au–Ag/Nafion/GCE in the absence and presence of Mel (1.0 mM). (B) Stability test: current variation for UA (1.0 mM), tested using the Au–Ag/Nafion/GCE in the absence and presence of Mel (1.0 mM), corresponding to the daily signal variation over 10 days.

Au–Ag NPs on the GCE surface at 5 μL, ideal for the optimal volume of Au–Ag NP solution in the present study.

PB solutions with different pH values and concentrations were evaluated as potential factors in the sensitivity of the sensor. As illustrated in Fig. 4C, the maximum current variation was obtained when the pH value of the PB solution was 7.0, which may be because higher pH values hinder the adsorption of UA (pKa 5.4) on the negatively charged HEPES Au–Ag NP surface (pKa 6.0–8.0 for HEPES). Furthermore, the effects of PB buffer concentrations in the range of 25–200 mM were tested (Fig. 4D), which revealed constant current variation within that range. Therefore, 50 mM PB (pH 7.0) was selected as the optimal condition for further investigations.

3.3. Sensitivity and selectivity

The sensitivity of the proposed electrochemical method for the detection of Mel was investigated using DPV under the optimal conditions to determine the anodic current response of UA at different Mel concentrations. The anodic peak current of UA decreased with an increasing concentration of Mel (Fig. 5A). A linear relationship was observed from the plot of current variation against Mel concentration in the range of 2.5–70 nM (R^2 = 0.947; inset in Fig. 5A). The proposed electrochemical method for the detection of Mel exhibited a LOD (signal-to-noise ratio = 3) of 1.8 nM, which indicated much

Table 2. ANOVA test of the decreasing rate of UA signal using the Au–Ag/Nafion/GCE for 10-day measurement.

Source of variation	Sum of squares	Degree of freedom	Mean square	F
Between days	0.006049	9	0.0006721	1.28
Within days	0.01053	20	0.0005265	
Total	0.016579	29		

Table 3. Parameters for the analysis of milk powder and cat food samples with Mel by using the proposed method.

Samples	Spiked Mel (nM)	Found Mel (nM)	Recovery (%)	RSD (n = 3) (%)
milk powder A	5	4.62	92.4	8.4
	10	9.49	94.9	8.9
	50	51.1	102.2	8.2
	70	70.5	94	7.9
milk powder B	5	4.79	95.8	8.5
	10	9.59	95.9	9.2
	50	49.9	99.8	9.3
	70	71.5	102.1	8.8
cat food	20	19.4	97	2.5
	30	31.1	103.7	3.1
	40	40.5	101.3	2.4
	50	47.9	95.9	1.7
	60	61.0	101.7	8.7

greater sensitivity than that of the standard approach for detecting permissible concentrations of Mel (20 μM) in food set by US FDA.

To investigate the selectivity of the proposed electrochemical method, Mel and other interference components (ammonia, phenylamine, KCl, NaCl, $CaCl_2$, $MgCl_2$, glucose, sucrose, lactose, fructose, glycine, adenine, and thymine (each 10 mM)) were individually added to UA solutions (1.0 mM). The anodic current was measured using the prepared Au–Ag/Nafion/GCE. As illustrated in Fig. 5B, only Mel induced significant current variation, indicating that the proposed electrochemical method provides excellent selectivity for Mel.

3.4. Reproducibility, stability, and practical applications

To assess the reproducibility of the prepared Au–Ag/Nafion/GCE, we measured the anodic current of UA (1.0 mM) in the absence and presence of Mel (1.0 mM) with 10 pieces of Au–Ag/Nafion/GCE (each electrode performed three cyclic voltammograms) and assessed the current variation. Fig. 6A displays the results of these experiments. The RSD was determined to be 14.2% from 10 different electrodes and 2.2%–9.3% within a single electrode. To test the stability (shelf life) of the prepared Au–Ag/Nafion/GCE, we evaluated the anodic current of UA (1.0 mM) in the absence and presence of Mel (1.0 mM) every day for 10 days and calculated the current variation (Fig. 6B). The RSD of the current variation was determined to be less than 7.1% for 10 days. For ANOVA, we selected a confidence level of 95%. The calculated F value was 1.28 (Table 2), which is less than the critical value of F (2.39). Therefore, there was no significant difference in the electrochemical performance of the prepared Au–Ag/Nafion/GCE over 10 days. These results indicated that the Au–Ag/Nafion/GCE could provide excellent electrochemical performance in terms of reproducibility and stability.

To validate the practicality of the proposed electrochemical method, the prepared Au–Ag/Nafion/GCE was used to detect Mel in milk powder and cat food samples. These samples were pretreated according to the procedure described in 2.6. Mass spectrometry did not reveal the presence of Mel in these samples. Table 3 displays the spiked concentration of Mel and recovery values for the Mel-free milk powder and cat food samples. The recovery values for the detection of Mel in milk powder A, milk powder B and cat food samples were 92.4%–102.2%, 95.8%–102.1%, and 95.9%–103.7%, respectively. Furthermore, the RSD values for the detection of Mel in milk powder A, milk powder B and cat food samples were 8.2%–8.9%, 8.5%–9.3%, and 1.7%–8.7%, respectively. These findings indicate that the proposed electrochemical method can achieve satisfactory reproducibility for the detection of Mel in milk powder and cat food samples without being influenced by the sample matrix.

4. Conclusions

We demonstrated a simple electrochemical method for the detection of Mel. The proposed method is based on the competitive adsorptive behavior of Mel on a Au–Ag/Nafion/GCE, which induces suppression of the anodic response of UA. We observed a LOD of 1.8 nM for Mel, which is significantly lower than the 20-μM limit permitted by the US FDA for food. Advantages of the reported method are the simplicity of the fabrication procedure of the Au–Ag/Nafion/GCE and measurement reproducibility and stability. The prepared Au–Ag/Nafion/GCE was employed to detect Mel in milk powder and cat food samples, with recovery ranging from 92.4% to 103.7%.

Conflicts of interest

The authors of the manuscript declare that there is no conflict of interest regarding the publication of this study.

Acknowledgements

This study was supported by the Ministry of Science and Technology of Taiwan under contract (MOST 108-2113-M-018-003). We thank Wallace Academic Editing for the English language editing.

References

[1] Tyan YC, Yang MH, Jong SB, Wang CK, Shiea J. Melamine contamination. Anal Bioanal Chem 2009;395:729–35.
[2] Chu PWS, Chan KM, Cheung STC, Wong YC. Review of analytical techniques used in proficiency-testing programs for melamine in animal feed and milk. Trac Trends Anal Chem 2010;29:1014–26.
[3] Sun FX, Ma W, Xu LG, Zhu YY, Liu LQ, Peng CF, et al. Analytical methods and recent developments in the detection of melamine. Trac Trends Anal Chem 2010;29:1239–49.
[4] Liu Y, Todd EED, Zhang Q, Shi JR, Liu XJ. Recent developments in the detection of melamine. J Zhejiang Univ - Sci B 2012;13:525–32.
[5] Rovina K, Siddiquee S. A review of recent advances in melamine detection techniques. J Food Compos Anal 2015; 43:25–38.
[6] Peris-Vicente J, Albiol-Chiva J, Roca-Genoves P, Esteve-Romero J. Advances on melamine determination by micellar liquid chromatography: a review. J Liq Chromatogr Relat Technol 2016;39:325–38.
[7] Lu Y, Xia YQ, Liu GZ, Pan MF, Li MJ, Lee NA, et al. A review of methods for detecting melamine in food samples. Crit Rev Anal Chem 2017;47:51–66.
[8] Nascimento CF, Santos PM, Pereira ER, Rocha FRP. Recent advances on determination of milk adulterants. Food Chem 2017;221:1232–44.
[9] Poonia A, Jha A, Sharma R, Singh HB, Rai AK, Sharma N. Detection of adulteration in milk: a review. Int J Dairy Technol 2017;70:23–42.
[10] Chen Q, Qie MF, Peng XS, Chen Y, Wang YL. Immunochromatographic assay for melamine based on luminescent quantum dot beads as signaling probes. RSC Adv 2020;10: 3307–13.
[11] Hu XJ, Song SFD, Zhu ZK, Lai ZJ, Gao Y, Koh K, et al. Visual detection of melamine in urine based on an AuNPs-curcumin system. Bull Chem Soc Jpn 2019;92:1275–9.
[12] Huang C, Lu FF, Xu K, Ding GJ, You LJ, Wang JB, et al. Synthesis of magnetic polyphosphazene-Ag composite particles as surface enhanced Raman spectroscopy substrates for the detection of melamine. Chin Chem Lett 2019;30: 2009–12.
[13] Inamuddin Kanchi S. One-pot biosynthesis of silver nanoparticle using Colocasia esculenta extract: colorimetric detection of melamine in biological samples. J Photochem Photobiol Chem 2020;391:112310.
[14] Li ZY, Li Y, Li L, Wang TY. Aquamarine blue emitting silver nanoparticles as fluorescent sensor for melamine detection. Spectroc Acta Pt A-Molec Biomolec 2019;217:51–9.
[15] Liu SJ, Kannegulla A, Kong XM, Sun R, Liu Y, Wang R, et al. Simultaneous colorimetric and surface-enhanced Raman scattering detection of melamine from milk. Spectroc Acta Pt A-Molec Biomolec 2020;231:118130.
[16] Miao YM, Wang RR, Sun XJ, Yan GQ. Preparation of DNA functional phosphorescent quantum dots and application in melamine detection in milk. RSC Adv 2019;9:21147–54.
[17] Mu WY, Huang PZ, Chen QY, Wang W. Determination of melamine and melamine-Cu(II) complexes in milk using a DNA-Ag hydrocolloid as the sensor. Food Chem 2020;311: 125889.
[18] Wang HB, Bai HY, Mao AL, Gan T, Liu YM. Poly(adenine)-templated fluorescent Au nanoclusters for the rapid and sensitive detection of melamine. Spectroc Acta Pt A-Molec Biomolec 2019;219:375–81.
[19] Xiao GN, Li L, Yan AM, He XY. Direct detection of melamine in infant formula milk powder solution based on SERS effect of silver film over nanospheres. Spectroc Acta Pt A-Molec Biomolec 2019;223:117269.
[20] Xu L, Li DX, Jiang BY, Xiang Y, Yuan R. Melamine-mediated base mismatch for label-free and amplified sensitive fluorescent detection of melamine in milk. Food Anal Meth 2019; 12:1255–61.
[21] Zhao N, Li HF, Tian CW, Xie YR, Feng ZB, Wang ZL, et al. Bioscaffold arrays decorated with Ag nanoparticles as a SERS substrate for direct detection of melamine in infant formula. RSC Adv 2019;9:21771–6.
[22] Guo MN, Liu SY, Wang MM, Lv YF, Shi JL, Zeng Y, et al. Double surfactants-assisted electromembrane extraction of cyromazine and melamine in surface water, soil and cucumber samples followed by capillary electrophoresis with contactless conductivity detection. J Sci Food Agric 2020;100: 301–7.
[23] Ritota M, Manzi P. Melamine detection in milk and dairy products: traditional analytical methods and recent developments. Food Anal Meth 2018;11:128–47.
[24] Li H, Somerson J, Xia F, Plaxco KW. Electrochemical DNA-based sensors for molecular quality control: continuous, real-time melamine detection in flowing whole milk. Anal Chem 2018;90:10641–5.
[25] Liu XJ, Song MM, Li F. Triplex DNA-based bioanalytical platform for highly sensitive homogeneous electrochemical detection of melamine. Sci Rep 2017;7:4490.
[26] Regasa MB, Soreta TR, Femi OE, Ramamurthy PC. Development of molecularly imprinted conducting polymer composite film-based electrochemical sensor for melamine detection in infant formula. ACS Omega 2020;5: 4090–9.
[27] Regasa MB, Soreta TR, Femi OE, Ramamurthy PC, Kumar S. Molecularly imprinted polyaniline molecular receptor-based chemical sensor for the electrochemical determination of melamine. J Mol Recogn 2020;33:e2836.
[28] Regasa MB, Soreta TR, Femi OE, Ramamurthy PC, Subbiahraj S. Novel multifunctional molecular recognition

elements based on molecularly imprinted poly (aniline-co-itaconic acid) composite thin film for melamine electrochemical detection. Sen Bio-Sen Res 2020;27:100318.
[29] Shellaiah M, Sun KW. Review on nanomaterial-based melamine detection. Chemosensors 2019;7:9.
[30] Daizy M, Tarafder C, Al-Mamun R, Liu XH, Aly MAS, Khan ZH. Electrochemical detection of melamine by using reduced graphene oxide-copper nanoflowers modified glassy carbon electrode. ACS Omega 2019;4:20324–9.
[31] Peng J, Feng Y, Han XX, Gao ZN. Sensitive electrochemical detection of melamine based on gold nanoparticles deposited on a graphene doped carbon paste electrode. Anal Methods 2016;8:2526–32.
[32] Ren QX, Shen XY, Sun YY, Fan RH, Zhang J. A highly sensitive competitive immunosensor based on branched polyethyleneimine functionalized reduced graphene oxide and gold nanoparticles modified electrode for detection of melamine. Food Chem 2020;304:125397.